Università degli studi di Padova
Dipartimento di Fisica e Astronomia

Tesi di Dottorato

Search for heavy resonances decaying into a Z boson and a vector boson in the $\nu\bar{\nu}\,q\bar{q}$ final state at CMS

Supervisor: Prof. Franco Simonetto
Candidate: Lisa Benato

Scuola di Dottorato di Ricerca, XXX ciclo

"I have no special talent. I am only passionately curious."
(A. Einstein)

Contents

1

Abstract

2

3

Chapter

1

Introduction

Chapter

2

Theoretical motivation

Chapter

3

The Large Hadron Collider and the CMS experiment

Chapter

4

Search for diboson resonances in the $ZV \to \nu\bar{\nu}q\bar{q}$ final state

4.1 Analysis overview

This analysis searches for signal of heavy resonances decaying into a pair of heavy vector bosons, using the data collected by the CMS experiment during 2016, for an integrated luminosity of $\mathcal{L} = 35.9\ \text{fb}^{-1}$. One Z boson is identified through its invisible decay ($\nu\nu$), while the other boson, labelled as V and consisting either as a W or a Z boson, is required to decay hadronically into a pair of quarks. The decay products (the bosons) of heavy (around the TeV scale) resonances are produced with large Lorentz boosts; as a consequence, the decay products of the bosons (quarks and neutrinos) are expected to be highly energetic and collimated. In this regime, the standard jet reconstruction algorithms fail in distinguishing the two jets from the quarks, suggesting to look for a signature composed of a large-cone high-p_T jet, in which both q and $\bar{q}$ lie, recoiling against a large amount of missing transverse energy ($\vec{p}_T^{\,\text{miss}}$) due to the neutrinos escaping the detector. The hadronically decaying boson (Z, W) is then reconstructed as one large-cone jet, whose mass is used to define the signal region and signal-depleted control regions, the sidebands. Jet substructure techniques are exploited in order to suppress background contamination and to classify the events in two exclusive signal purity categories, allowing to improve the discovery reach.

A ZZ final state, predicted by the bulk graviton model (sec. **??**), can be reconstructed in channels with high purity but limited statistics (four charged leptons) and large statistics but overwhelming backgrounds (no charged leptons). The choice to look for one boson decaying hadronically and the other Z into neutrinos represents the best compromise between these two extremes. This topology can be also utilized to reconstruct a charged spin-1 vector boson decaying into an invisible Z and a hadronic W, predicted by HVT model (sec. **??**), making this analysis sensitive to a generic VZ final state.

Signal events are collected with trigger paths requiring high $\vec{p}_T^{\,\text{miss}}$ recoiling against jet activity. This signature is clearly a very challenging one in an environment with more than 50 primary collisions per bunch crossing. For this reason, the Particle-Flow algorithm is run at trigger level to obtain the highest possible resolution on the jets and thus on the $\vec{p}_T^{\,\text{miss}}$.

The search is performed by examining the distribution of the diboson reconstructed transverse mass of the resonance VZ (m_{VZ}^T) for a localized excess. The shape and normalization of the main

background of the analysis (namely, the production of an electroweak boson in association with jets) are estimated with a data-simulation hybrid approach using the distribution of data in the sidebands, corrected for a function accounting for potential differences between the signal region and the sidebands, while the minor background sources are taken from simulations.
In fig. 4.1, a typical signal event of the $W' \to WZ \to q\bar{q}'\nu\bar{\nu}$ process detected by the CMS experiment is displayed; the mass of the W' is 2.5 TeV. The muon chambers in the barrel (DTs, in light red) and in the endcaps (CSCs, in light blue), along with the tracker detector (green) are shown in the (r,ϕ) transverse plane (left) and the (r,z) longitudinal plane (right). The large-cone jet, identifying the W hadronic decay, is displayed in red; the energy deposits in ECAL (light orange) and in HCAL (in violet) can be seen in the picture. The missing transverse energy, signature of the Z invisible decay, is represented as a blue arrow, lying in the transverse plane. The track multiplicity (green tracks) is shown in the center of the detector, where the tracker is installed.

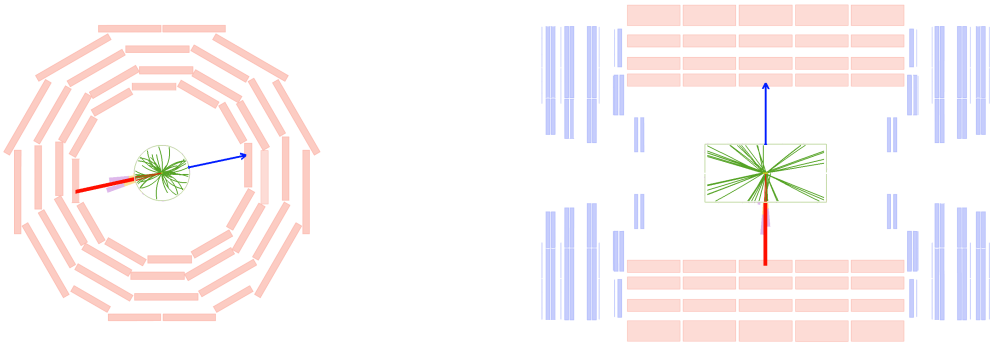

Figure 4.1: Left: representation of the decay of a W' of mass 2.5 TeV, in the transverse plane of the CMS detector. Right: representation of the decay of a W' of mass 2.5 TeV, in the longitudinal plane of the CMS detector.

4.2 Data and Monte Carlo simulations samples

4.2.1 Signal samples

Signal samples of a spin-2 (Bulk Graviton) decaying in a pair of Z bosons are exploited in the analysis. To target the final state, one of the two Z bosons is forced to decay into neutrinos, while the other Z is forced to decay hadronically. The signal samples are produced in the narrow-width approximation by setting the resonance with to 0.1% of its mass. Twelve mass points with 100000 events each are simulated, with a m_G ranging from 600 GeV up to 4500 GeV.
Additionally, samples of a spin-1 HVT-like W' resonance decaying in a Z boson and a W boson are studied. The Z boson is forced to decay into neutrinos, and the W boson is forced to decay hadronically. Also in this case the signal samples are produced in the narrow-width approximation by setting the resonance with to 0.1% of its mass. Twelve mass points with 100000 events each are simulated, with a $m_{W'}$ ranging from 600 GeV up to 4500 GeV.
The signal samples are generated at leading-order (LO) with the MADGRAPH5_AMCATNLO v 2.2.2 [1] matrix element generator, while hadronization and fragmentation are handled by PYTHIA 8 [2] version 8.2121 with CUETP8M1 [3] tuning. A full detector simulation and event reconstruction has been performed with GEANT4 [4] and CMSSW. The detector alignement scenario, calibrations and pile-up distributions are generated according to the expectations in 2016 data.
All the signal samples used in the analysis and the related properties are reported in Tables 4.1-4.2.

Signal process	m_G	Events	$\sigma \times \mathscr{B}$ (pb)
$G \to ZZ \to q\bar{q}\nu\bar{\nu}$	600 GeV	100000	0.27964
$G \to ZZ \to q\bar{q}\nu\bar{\nu}$	800 GeV	100000	0.27964
$G \to ZZ \to q\bar{q}\nu\bar{\nu}$	1000 GeV	100000	0.27964
$G \to ZZ \to q\bar{q}\nu\bar{\nu}$	1200 GeV	100000	0.27964
$G \to ZZ \to q\bar{q}\nu\bar{\nu}$	1400 GeV	100000	0.27964
$G \to ZZ \to q\bar{q}\nu\bar{\nu}$	1800 GeV	100000	0.27964
$G \to ZZ \to q\bar{q}\nu\bar{\nu}$	2000 GeV	100000	0.27964
$G \to ZZ \to q\bar{q}\nu\bar{\nu}$	2500 GeV	100000	0.27964
$G \to ZZ \to q\bar{q}\nu\bar{\nu}$	3000 GeV	100000	0.27964
$G \to ZZ \to q\bar{q}\nu\bar{\nu}$	3500 GeV	100000	0.27964
$G \to ZZ \to q\bar{q}\nu\bar{\nu}$	4000 GeV	100000	0.27964
$G \to ZZ \to q\bar{q}\nu\bar{\nu}$	4500 GeV	100000	0.27964

Table 4.1: Spin-2 (Bulk Graviton) signal samples and production cross sections (assumed to be 1pb) multiplied by the respective branching fractions of the Z decays considered ($\mathscr{B}(Z \to \nu\nu) = 0.20$, $\mathscr{B}(Z \to qq) = 0.6991$).

Signal process	$m_{W'}$	Events	$\sigma \times \mathscr{B}$ (pb)
$W' \to WZ \to q\bar{q}'\nu\bar{\nu}$	600 GeV	100000	0.13482
$W' \to WZ \to q\bar{q}'\nu\bar{\nu}$	800 GeV	100000	0.13482
$W' \to WZ \to q\bar{q}'\nu\bar{\nu}$	1000 GeV	100000	0.13482
$W' \to WZ \to q\bar{q}'\nu\bar{\nu}$	1200 GeV	100000	0.13482
$W' \to WZ \to q\bar{q}'\nu\bar{\nu}$	1400 GeV	100000	0.13482
$W' \to WZ \to q\bar{q}'\nu\bar{\nu}$	1800 GeV	100000	0.13482
$W' \to WZ \to q\bar{q}'\nu\bar{\nu}$	2000 GeV	100000	0.13482
$W' \to WZ \to q\bar{q}'\nu\bar{\nu}$	2500 GeV	100000	0.13482
$W' \to WZ \to q\bar{q}'\nu\bar{\nu}$	3000 GeV	100000	0.13482
$W' \to WZ \to q\bar{q}'\nu\bar{\nu}$	3500 GeV	100000	0.13482
$W' \to WZ \to q\bar{q}'\nu\bar{\nu}$	4000 GeV	100000	0.13482
$W' \to WZ \to q\bar{q}'\nu\bar{\nu}$	4500 GeV	100000	0.13482

Table 4.2: Spin-1 (W') signal samples and production cross sections (assumed to be 1pb) multiplied by the Z and W branching fraction ($\mathscr{B}(Z \to \nu\nu) = 0.2$, $\mathscr{B}(W \to qq) = 0.6760$).

4.2.2 Signal characterization

This analysis is performed in a high mass region (from 1 TeV to 4.5 TeV). The MADGRAPH algorithm generates the hard process production in the collision with $p_T = 0$. In the next step of the simulation, during the hadronization, PYTHIA adds the QCD ISR (initial state radiation) and consequently a resonance p_T different from 0. Kinematical distributions at generator level are showed in fig. 4.2-4.4 for spin-2 Bulk Graviton signal, and in fig. 4.5-4.7 for spin-1 HVT W' signal.

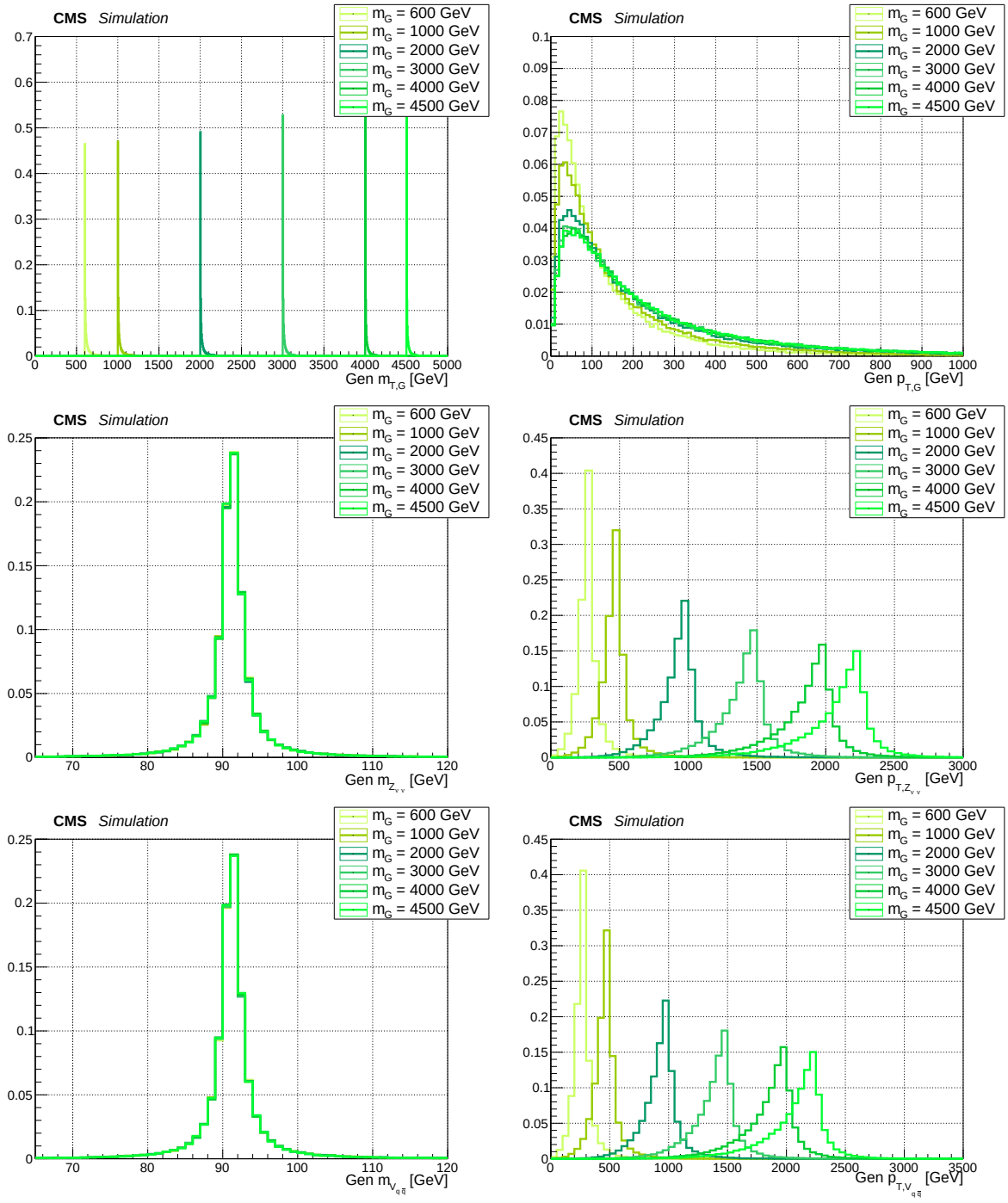

Figure 4.2: Main signal kinematic quantities at generation level after parton showering, for spin-2 Bulk Graviton signal, considering different mass hypoteses ($m_G = 0.6, 1, 2, 3, 4, 4.5$ TeV). Top: graviton transverse mass and p_T distributions. Center: invisibly decaying Z mass and p_T. Bottom: hadronically decaying Z mass and p_T.

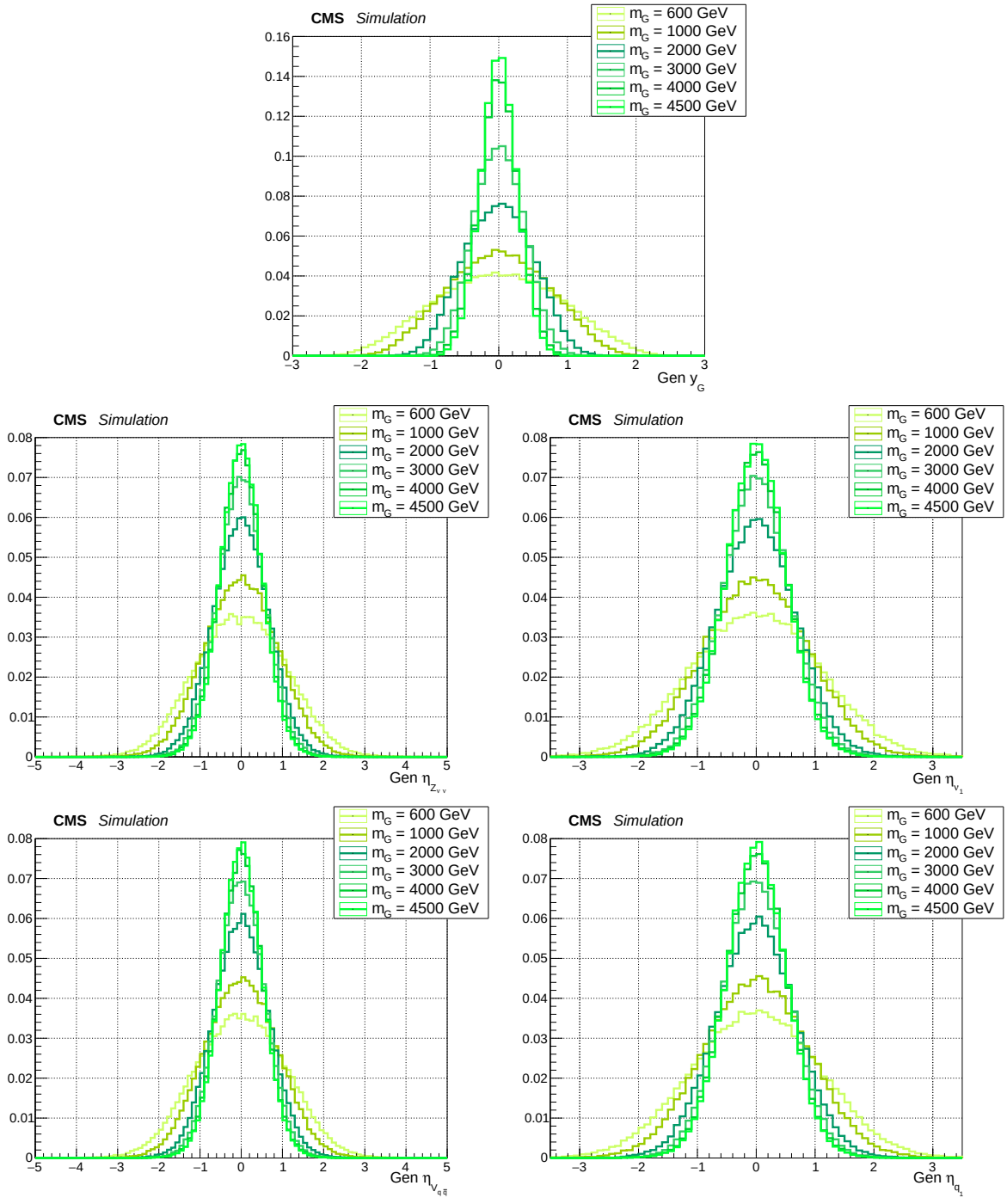

Figure 4.3: Main signal kinematic quantities at generation level after parton showering, for spin-2 Bulk Graviton signal, considering different mass hypoteses ($m_G = 0.6, 1, 2, 3, 4, 4.5$ TeV). Top: graviton rapidity $\mathscr{Y}$. Center: pseudorapidity η of the invisibly decaying Z, and pseudorapidity of the leading neutrino. Bottom: pseudorapidity η of the hadronically decaying Z, and pseudorapidity of the leading quark.

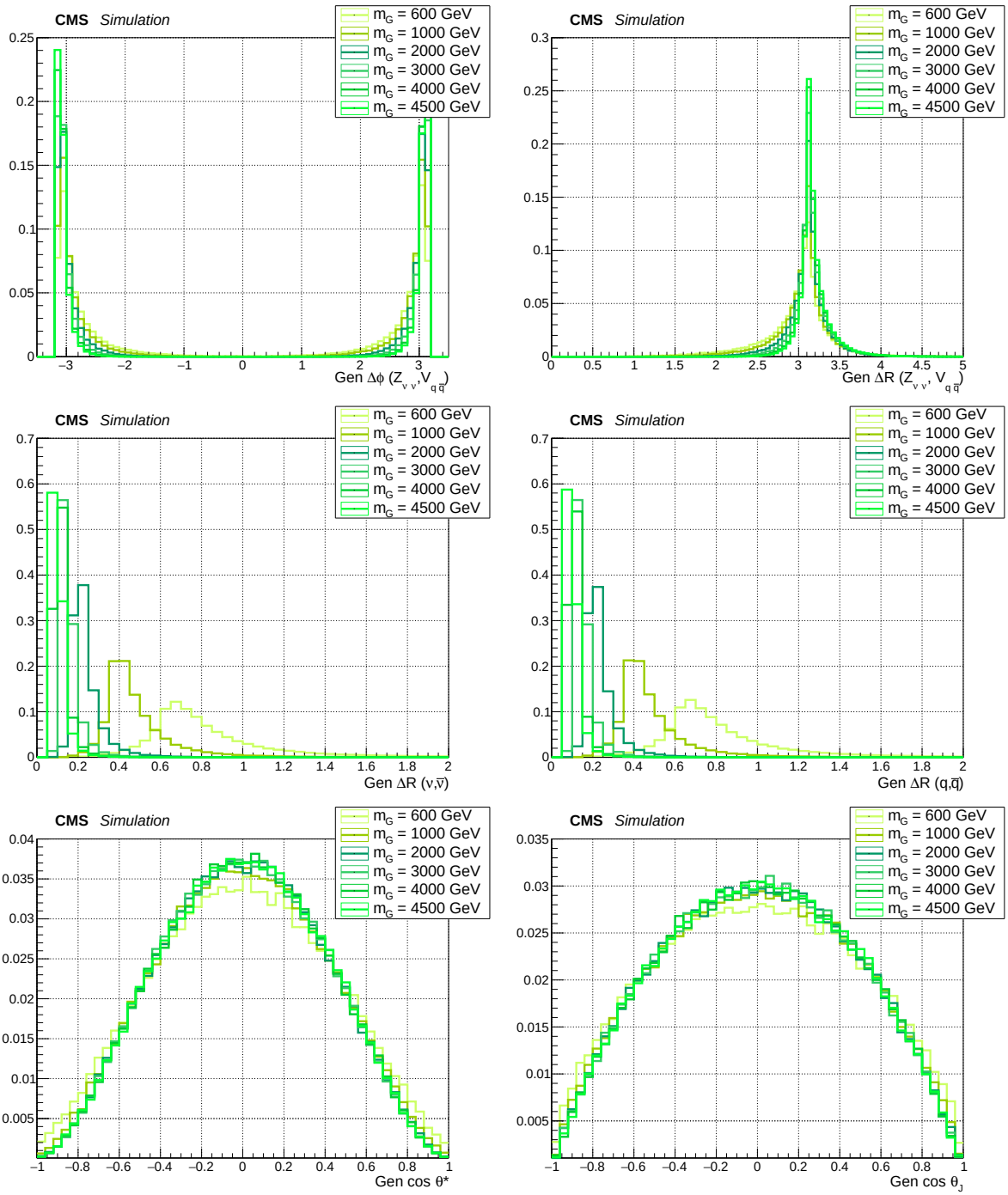

Figure 4.4: Main signal kinematic quantities at generation level after parton showering, for spin-2 Bulk Graviton signal, considering different mass hypoteses ($m_G = 0.6, 1, 2, 3, 4, 4.5$ TeV). Top: angular separation in the transverse plane $\Delta\phi$ (left) and solid angle ΔR (right) between leptonic Z and hadronic Z. Center: solid angle between the neutrinos and the quarks. Bottom: distribution of $\cos\theta^*$ and $\cos\theta_J$ (described in text).

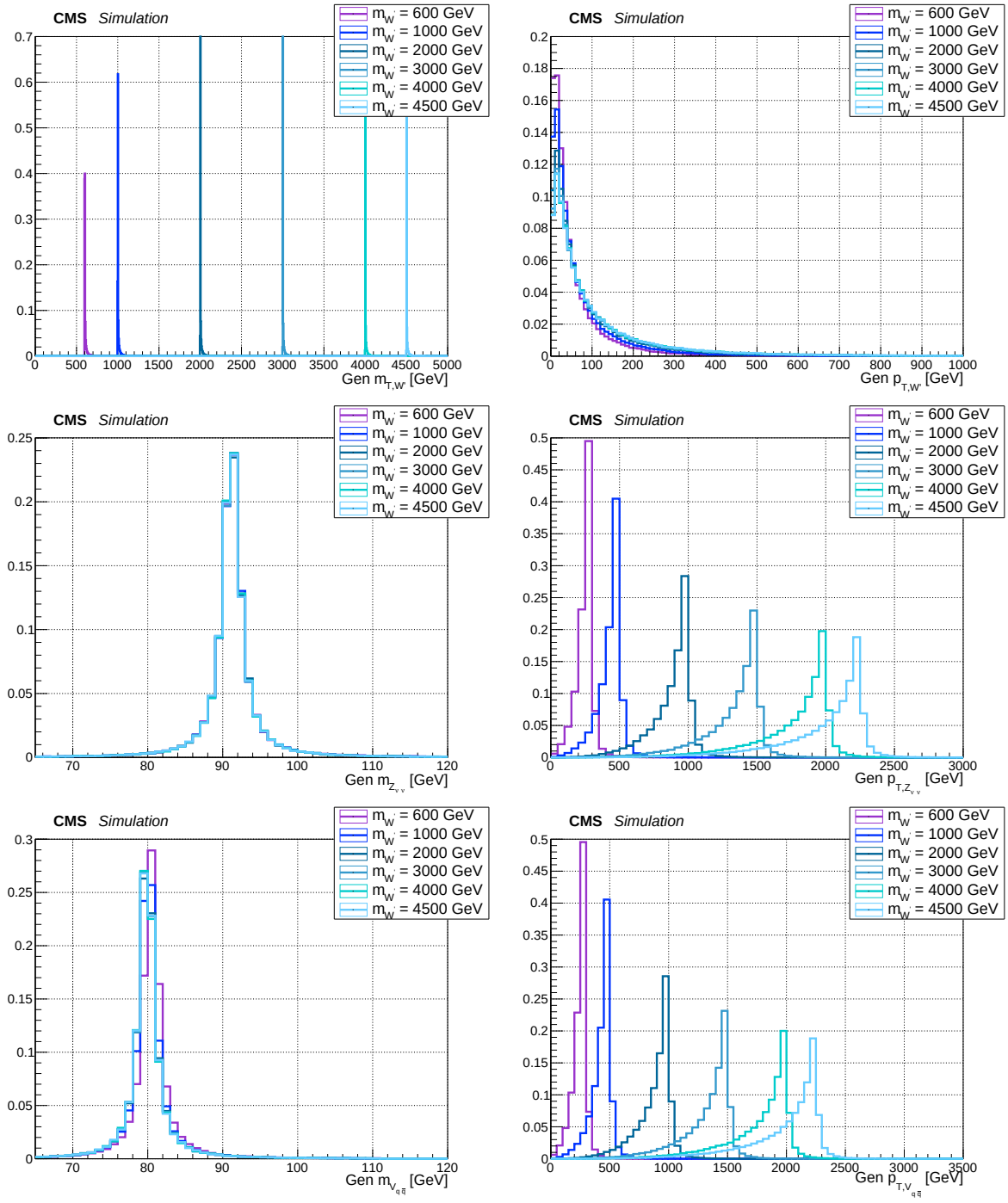

Figure 4.5: Main signal kinematic quantities at generation level after parton showering, for spin-1 W' signal, considering different mass hypoteses ($m_{W'} = 0.6, 1, 2, 3, 4, 4.5$ TeV). Top: W' transverse mass and p_T distributions. Center: invisibly decaying Z mass and p_T. Bottom: hadronically decaying W mass and p_T.

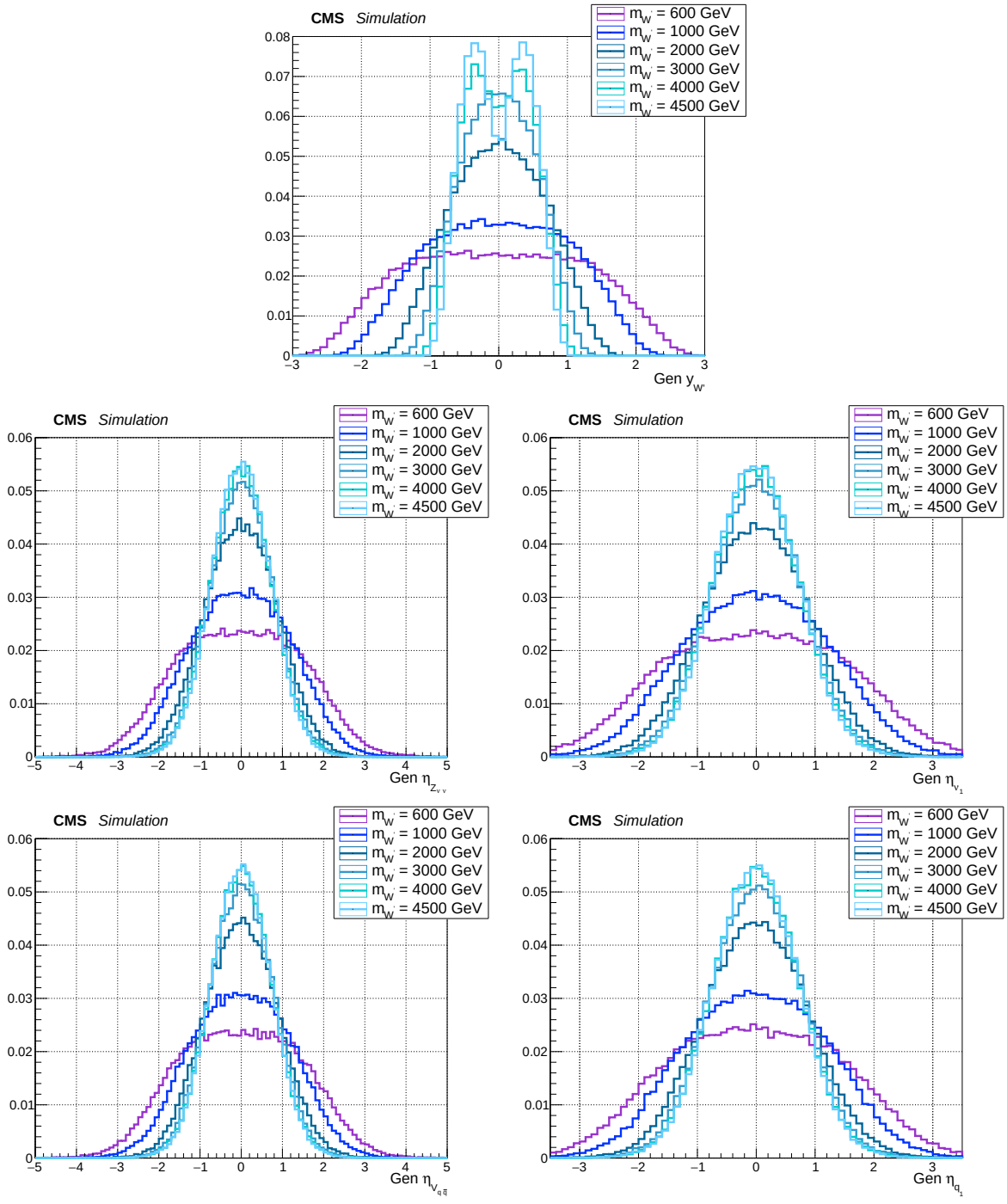

Figure 4.6: Main signal kinematic quantities at generation level after parton showering, for spin-1 W' signal, considering different mass hypoteses ($m_{W'} = 0.6, 1, 2, 3, 4, 4.5$ TeV). Top: W' rapidity $\mathcal{Y}$. Center: pseudorapidity η of the invisibly decaying Z, and pseudorapidity of the leading neutrino. Bottom: pseudorapidity η of the hadronically decaying W, and pseudorapidity of the leading quark.

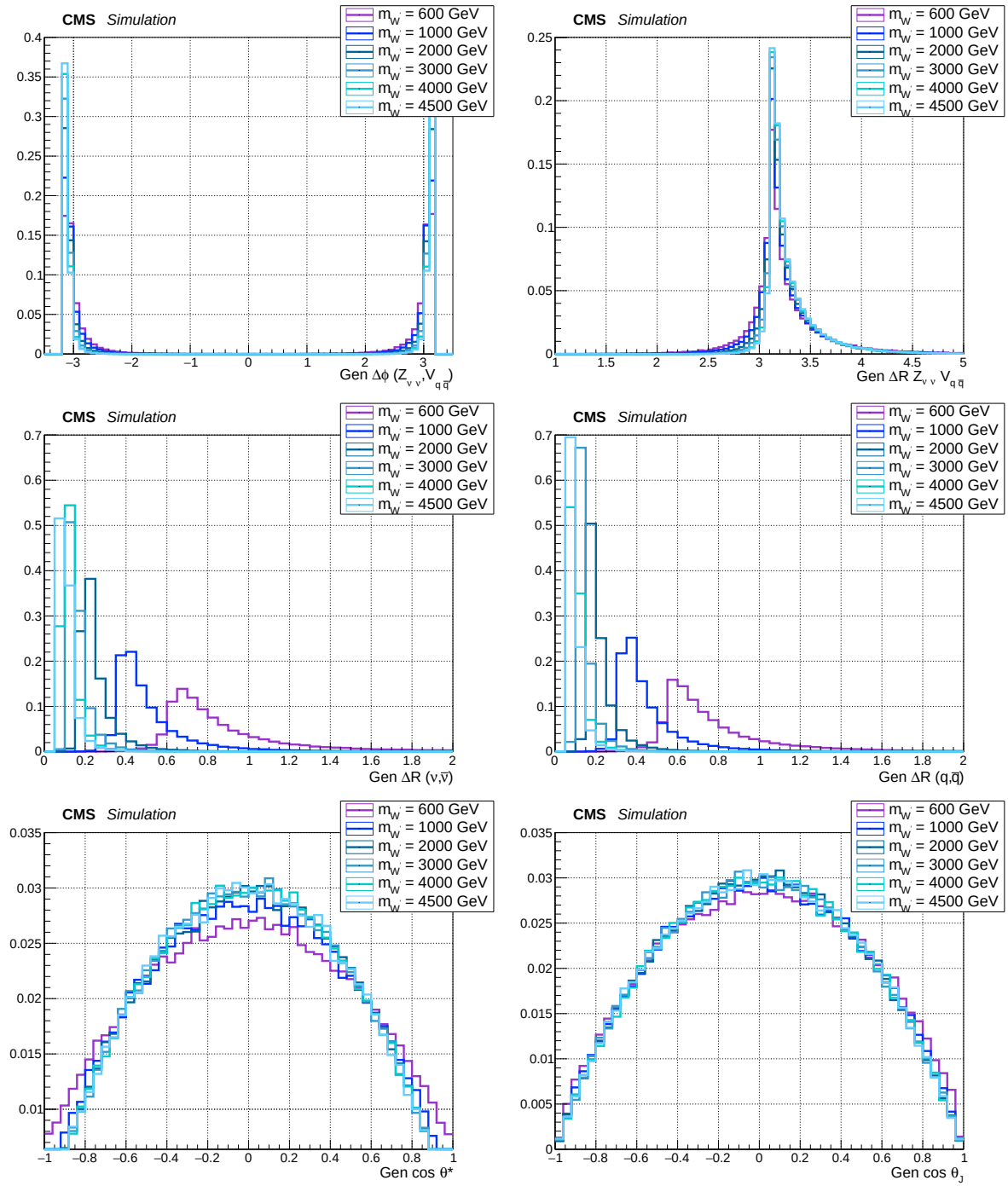

Figure 4.7: Main signal kinematic quantities at generation level after parton showering, for spin-1 W' signal, considering different mass hypoteses ($m_{W'} = 0.6, 1, 2, 3, 4, 4.5$ TeV). Top: angular separation in the transverse plane $\Delta\phi$ (left) and solid angle ΔR (right) between leptonic Z and hadronic W. Center: solid angle between the neutrinos and the quarks. Bottom: distribution of $\cos\theta^*$ and $\cos\theta_J$ (described in text).

Angular distributions are related to the spin, the polarization and the kinematics of the produced resonance; in particular:

- the ΔR among neutrinos and quarks reflect the boosted nature of the electroweak bosons: the more massive the resonance, the larger the boost, and hence the closer the fermions. By looking at fig. 4.4-4.7, with a jet clustering parameter of 0.8 (AK8 jet) it is possible to enclose the quarks produced by the decay of the V boson, for a resonance mass over 1 TeV;

- the $\cos\theta^*$, namely the cosine of the angle between the momentum of the V boson, calculated in the resonance rest frame, and the flight direction of the resonance itself in the laboratory frame. This variable depends on the spin of the diboson resonance (spin-2 and spin-1 distributions are different, fig. 4.4-4.7).

- the $\cos\theta_J$, the cosine of the angle between the momentum of the leading quark, calculated in the V rest frame, and the flight direction of the V boson in the laboratory frame. This variable depends on the polarization state of the decay bosons [5]; in both HVT and bulk graviton model, electroweak bosons are expected to be longitudinally polarized. When $\cos\theta_J \to 0$, quarks are produced very close in angle and hence it is difficult to disentangle the two substructures in the large-cone jet (sec. **??**); when $\cos\theta_J \to \pi$ the quarks are emitted asymmetrically (one is softer than the other).

4.2.3 Background samples

The physics processes yielding final states with two neutrinos in association with a pair of quarks are considered as sources of background; they are listed in tab. 4.3, along with the expected cross-sections at next-to-leading order (NLO) or next-to-next-to leading (NNLO).

- **Z + jets**: this process represents the main irreducible background for the signal. The production of single Z/γ^* bosons in association with one or more partons or gluons in the final state has a similar topology to the signal. This Z +jets background is produced in samples binned in p_T of the Z boson starting from 100 GeV with the aMC@NLO generator, with FXFX merging [6]. The contribution from events with $p_T < 100$ GeV is negligible after we require the $\vec{p}_T^{\,\text{miss}}$ to be greater than 200 GeV (sec. **??**).

- **W + jets**: the leptonic decay of a W boson can be an irreducible background in the case the charged lepton escapes undetected (e.g. outside the detector acceptance) or fails the lepton identification requirements. The production of a W boson has a cross section larger by an order of magnitude with respect to the Z, and this makes the W +jets a relevant background also when a lepton veto is applied. This W +jets background is produced in samples binned in p_T of the W boson starting from 100 GeV with the aMC@NLO generator.

- **top**: production of $t\bar{t}$ pairs represents a particularly challenging background at the LHC, given its large production cross section. These events always contain two energetic b-jets and two W bosons which may decay to leptons that escape the detector or fail to be identified as leptons. Inclusive $t\bar{t}$ decays have been considered. The primary handles to reduce the $t\bar{t}$ background are topological, such as the azimuthal opening angle between the Z boson and the dijet system, which is more broadly distributed in top pair production than in signal events. In $t\bar{t}$ production the dilepton mass is not resonating in the Z mass region, and their p_T spectrum is sharply falling, given the absence of a single boosted resonance. This analysis makes use of $t\bar{t}$ samples based on POWHEG v2 [7] NLO generator. Single-top and single-antitop samples are produced in the 5-flavours scheme using POWHEG v2 [8] NLO generator.

- **Diboson**: the production of two vector bosons in the SM is a rare process inducing and irreducible background for this search, with a similar kinematics to that of the signal. Inclusive diboson production processes (WW, WZ, ZZ) are considered.

Table 4.3: Simulated samples. The cross section × branching ratio is shown in pb. (*) cross sections taken from McM.

Signal process	Kinematical cuts	Generator	$\sigma \times \mathscr{B}$ [pb]	Events
$Z \to \nu\nu$ + jets	$100 < p_{T,Z} < 250$ GeV	amcatnloFXFX – Pythia8	170.4	5353639
$Z \to \nu\nu$ + jets	$100 < p_{T,Z} < 250$ GeV	amcatnloFXFX – Pythia8	170.4	5356674
$Z \to \nu\nu$ + jets	$250 < p_{T,Z} < 400$ GeV	amcatnloFXFX – Pythia8	6.636	1052985
$Z \to \nu\nu$ + jets	$250 < p_{T,Z} < 400$ GeV	amcatnloFXFX – Pythia8	6.636	1059634
$Z \to \nu\nu$ + jets	$400 < p_{T,Z} < 650$ GeV	amcatnloFXFX – Pythia8	0.9372	1050705
$Z \to \nu\nu$ + jets	$400 < p_{T,Z} < 650$ GeV	amcatnloFXFX – Pythia8	0.9372	1050592
$Z \to \nu\nu$ + jets	$p_{T,Z} > 650$ GeV	amcatnloFXFX – Pythia8	0.1042	1022595
$Z \to \nu\nu$ + jets	$p_{T,Z} > 650$ GeV	amcatnloFXFX – Pythia8	0.1042	1024620
$W \to \ell\nu$ + jets	$100 < p_{T,W} < 250$ GeV	amcatnloFXFX – Pythia8	676.3	10089661
$W \to \ell\nu$ + jets	$100 < p_{T,W} < 250$ GeV	amcatnloFXFX – Pythia8	676.3	10088599
$W \to \ell\nu$ + jets	$250 < p_{T,W} < 400$ GeV	amcatnloFXFX – Pythia8	23.94	1001250
$W \to \ell\nu$ + jets	$250 < p_{T,W} < 400$ GeV	amcatnloFXFX – Pythia8	23.94	1000132
$W \to \ell\nu$ + jets	$400 < p_{T,W} < 650$ GeV	amcatnloFXFX – Pythia8	3.031	951713
$W \to \ell\nu$ + jets	$400 < p_{T,W} < 650$ GeV	amcatnloFXFX – Pythia8	3.031	988234
$W \to \ell\nu$ + jets	$p_{T,W} < 650$ GeV	amcatnloFXFX – Pythia8	0.4524	989482
$W \to \ell\nu$ + jets	$p_{T,W} > 650$ GeV	amcatnloFXFX – Pythia8	0.4524	985127
$t\bar{t}$ inclusive	-	Powheg – Pythia8	831.76	77229341
t (tW channel) 5f inclusive	-	Powheg – Pythia8	35.85	6952830
$\bar{t}$ ($\bar{t}W$ channel) 5f inclusive	-	Powheg – Pythia8	35.85	6933094
t (s-channel) 4f lepton decays	-	amcatnloFXFX – Pythia8	3.344	622990
t (t-channel) 4f inclusive	-	Powheg – Madspin – Pythia8	136.02	67240808
$\bar{t}$ (t-channel) 4f inclusive	-	Powheg – Madspin – Pythia8	80.95	38811017
WW inclusive	-	Pythia8	118.7	994012
WW inclusive	-	Pythia8	118.7	6987124
WZ inclusive	-	Pythia8	47.2	1000000
WZ inclusive	-	Pythia8	47.2	2995828
ZZ inclusive	-	Pythia8	16.6	990064
ZZ inclusive	-	Pythia8	16.6	998034

4.2.4 V boson momentum corrections

4.2.4.1 NLO Electroweak

Corrections to the V p_T spectrum comes from NLO electroweak contributions, that are enhanced at TeV scale. These corrections are effectively applied on a per-event basis depending on the p_T of the vector boson at generation level. The calculation of these contributions is explained in Ref. [**?**]. Figure 4.8 shows the amount of the correction for the W and Z bosons.

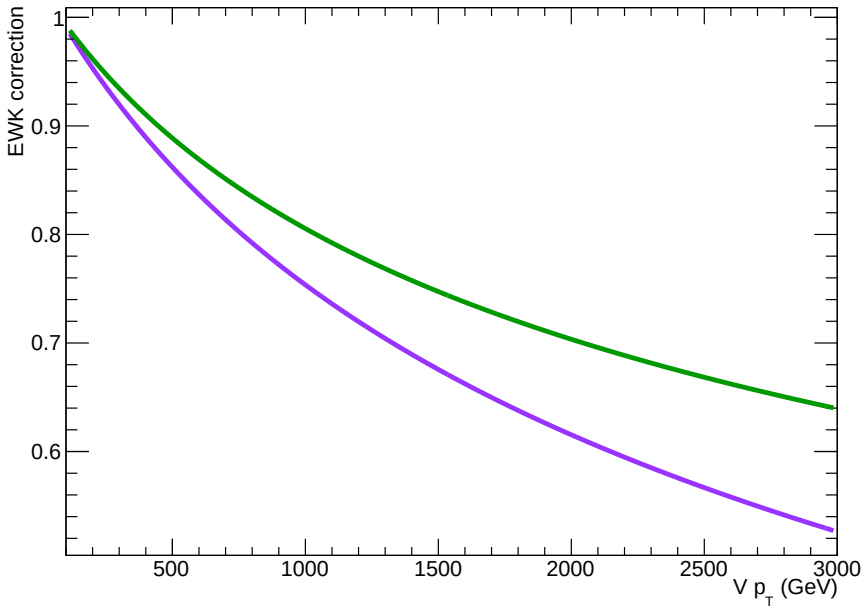

Figure 4.8: Electroweak corrections for the Z (green line) and W boson (purple line) as a function of the transverse momentum [**?**].

4.2.5 Data

Data samples used in this analysis have been collected during 2016 RunB, RunC, RunD, RunE, RunF, RunG and RunH, at a center-of-mass energy of 13 TeV, in 25ns runs and with the magnetic field enabled. The `MET` datasets are used for data selected with a $\vec{p}_T^{\,\text{miss}}$ trigger. `SingleMuon` and `SingleElectron` datasets are used to measure trigger efficiency on data. The full list of datasets used is shown in Table 4.4. Data is processed from `ReMiniAOD` campaign.

The JSON file used in the analysis is the following:

- **Golden**: `Cert_271036-284044_13TeV_23Sep2016ReReco_Collisions16_JSON.txt` includes all the runs certified as "good" for all subsystems. The integrated luminosity amounts to 35.867 fb^{-1}.

In order to remove problematic or noise-dominated events, the following list of filters [9](ICHEP version) have been applied on data and MC:

- `HBHENoiseFilter`
- `HBHENoiseIsoFilter`

- `EcalDeadCellTriggerPrimitiveFilter`
- `goodVertices`
- `eeBadScFilter` (not recommended for Monte Carlo, hence not applied)
- `globalTightHalo2016Filter`
- `BadPFMuonFilter`
- `BadChargedCandidateFilter`

Table 4.4: Datasets Run2016B-H.

Dataset
MET/Run2016B-03Feb2017-v2
MET/Run2016C-03Feb2017-v1
MET/Run2016D-03Feb2017-v1
MET/Run2016E-03Feb2017-v1
MET/Run2016F-03Feb2017-v1
MET/Run2016G-03Feb2017-v1
MET/Run2016H-03Feb2017_ver2-v1
MET/Run2016H-03Feb2017_ver3-v1
SingleMuon/Run2016B-03Feb2017-v2
SingleMuon/Run2016C-03Feb2017-v1
SingleMuon/Run2016D-03Feb2017-v1
SingleMuon/Run2016E-03Feb2017-v1
SingleMuon/Run2016F-03Feb2017-v1
SingleMuon/Run2016G-03Feb2017-v1
SingleMuon/Run2016H-03Feb2017_ver1-v1
SingleMuon/Run2016H-03Feb2017_ver2-v1
SingleElectron/Run2016B-03Feb2017-v2
SingleElectron/Run2016C-03Feb2017-v1
SingleElectron/Run2016D-03Feb2017-v1
SingleElectron/Run2016E-03Feb2017-v1
SingleElectron/Run2016F-03Feb2017-v1
SingleElectron/Run2016G-03Feb2017-v1
SingleElectron/Run2016H-03Feb2017_ver2-v1
SingleElectron/Run2016H-03Feb2017_ver3-v1

4.2.6 Trigger

Events are selected on-line by a two-stage trigger. The Level 1 (L1) trigger consists of hardware processors that perform a very basic selection and counting of physics objects, and reduce the rate from 40 MHz down to 100 kHz. Events passing the L1 decision are acquired by the DAQ system, and a complete and more accurate reconstruction is performed by the High Level Trigger (HLT), which exploits similar but faster variations of the same algorithms used in the offline event reconstruction. A trigger path is a string that identifies a list of selections performed at HLT. $\vec{p}_T^{\,\text{miss}}$ triggers have been used in this analysis: they are the logic OR of different trigger quantities, with thresholds on both the $\vec{p}_T^{\,\text{miss}}$ and the H_T^{miss} computed using particle flow objects.

The list of triggers used, along with the L1 seeds, is reported in Table 4.5.

Table 4.5: HLT trigger paths used in the analysis.

HLT path	L1 seeds
HLT_PFMETNoMu90_PFMHTNoMu90_IDTight	L1_ETM70 OR L1_DoubleJetC56_ETM60 OR L1_ETM60 OR L1_ETM50
HLT_PFMETNoMu110_PFMHTNoMu110_IDTight	L1_ETM70 OR L1_DoubleJetC56_ETM60 OR L1_ETM60 OR L1_ETM50
HLT_PFMETNoMu120_PFMHTNoMu120_IDTight	L1_ETM70 OR L1_DoubleJetC56_ETM60 OR L1_ETM60 OR L1_ETM50
HLT_PFMET170_NoiseCleaned or	L1_ETM60 OR L1_ETM70
HLT_PFMET170_JetIdCleaned or	L1_ETM60 OR L1_ETM70
HLT_PFMET170_HBHECleaned	L1_ETM60 OR L1_ETM70

The approach adopted in this analysis consists in calculating the trigger efficiency on data, and applying the measured efficiency to Monte Carlo samples. Therefore the trigger is not required to have fired in MC.

The efficiency of the $\vec{p}_T^{\,\text{miss}}$ triggers is measured on SingleMuon dataset by selecting $W \to \mu\nu$ events using a single muon trigger (HLT_IsoMu24 OR HLT_IsoTkMu24_v), asking to have one isolated TightId muon, with the suitable p_T threshold to be in the plateu of the muon trigger. The efficiency has been calculated as a function of the minimum quantity between the offline reconstructed missing transverse momentum, where the contribution of the muon is subtracted from the $\vec{p}_T^{\,\text{miss}}$ computation as in the online algorithm, and the offline H_T^{miss}, defined as $H_T^{\text{miss}} = \sum_j^{\text{n. of AK4 jets}} p_T^j$. This approach guarantees to mimic the behaviour of the online L1 trigger seeds. The detailed selections:

- HLT_IsoMu24_v OR HLT_IsoTkMu24_v
- 1 muon, tight ID, $p_T > 35$ GeV, tight isolation
- at least one AK8 jet, $p_T > 170$ GeV, $|\eta| < |2.5$, LooseID
- AK4 jets included in H_T^{miss}: $p_T > 30$ GeV, $|\eta| < |2.5$, LooseID

The efficiency of the $\vec{p}_T^{\,\text{miss}}$ triggers has independently been measured also on SingleElectron dataset, by selecting $W \to e\nu$ events using a single electron trigger (HLT_Ele27_WPLoose_Gsf OR HLT_Ele27_WPTight_GsfOR HLT_Ele32_WPTight_Gsf), asking to have one TightId electron,

with the suitable p_T threshold, and asking to the electron and the $\vec{p}_T^{\,\text{miss}}$ to be separated in ϕ in order to suppress fake events ($\Delta\phi > 0.5$).

- `HLT_Ele27_WPLoose_Gsf OR HLT_Ele27_WPTight_GsfOR HLT_Ele32_WPTight_Gsf`
- 1 electron, tight ID, $p_T > 35$ GeV
- at least one AK8 jet, $p_T > 170$ GeV, $|\eta| < |2.5$, LooseID
- AK4 jets included in H_T^{miss}: $p_T > 30$ GeV, $|\eta| < |2.5$, LooseID

The full available statistics has been employed to derive the efficiency. The final turn-on curve for the $\vec{p}_T^{\,\text{miss}}$ trigger used in this analysis is shown in fig.4.9-4.10, divided in muon-electron dataset. The `METNoMu` trigger efficiencies are displayed separately, together with their OR. The quantity plotted in the x axis depends on the dataset, according to what was explained previously.

The difference needed to cover the gap between these two curves is taken as trigger systematic uncertainty, and it amounts to 1% at 200 GeV.

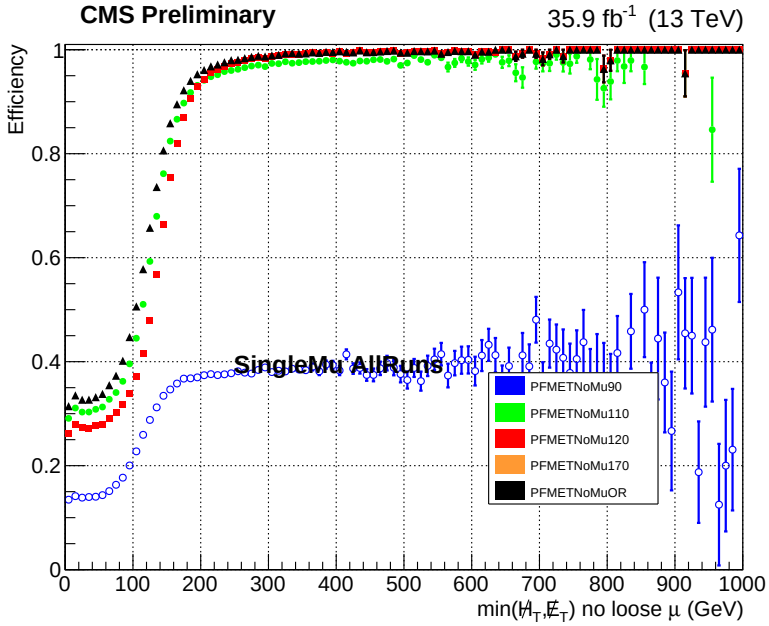

Figure 4.9: $\vec{p}_T^{\,\text{miss}}$ trigger efficiency for the $\vec{p}_T^{\,\text{miss}}$ trigger paths used in this analysis, calculated on `SingleMuon` dataset.

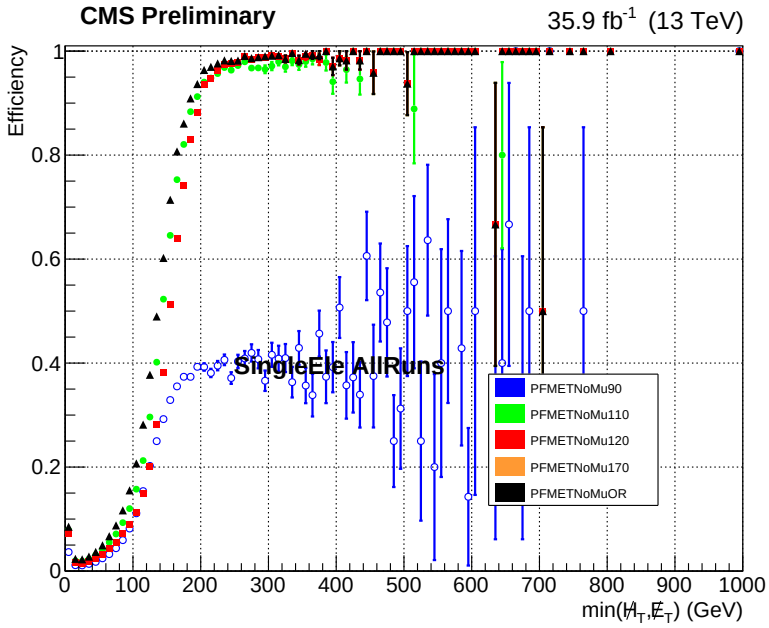

Figure 4.10: $\vec{p}_T^{\,\text{miss}}$ trigger efficiency for the $\vec{p}_T^{\,\text{miss}}$ trigger paths used in this analysis, calculated on `SingleElectron` dataset.

Chapter

5

Conclusions

Plot di Clemens

Bibliography

[1] J. Alwall et al., *The automated computation of tree-level and next-to-leading order differential cross sections, and their matching to parton shower simulations*, *JHEP* **07** (2014) 079, [1405.0301].

[2] Torbjorn Sjostrand and Stephen Mrenna and Peter Skands, *A brief introduction to pythia 8.1*, *Comput.Phys.Commun.* **178** (2008) 852–867, [0710.3820].

[3] CMS collaboration, CMS Collaboration, *Event generator tunes obtained from underlying event and multiparton scattering measurements*, *Eur. Phys. J.* **C** (2016) 155, [1512.00815].

[4] S. Agostinelli, J. Allison, K. Amako, J. Apostolakis, H. Araujo, P. Arce et al., *Geant4a simulation toolkit*, *Nuclear Instruments and Methods in Physics Research Section A: Accelerators, Spectrometers, Detectors and Associated Equipment* **506** (2003) 250 – 303.

[5] CMS collaboration, V. Khachatryan et al., *Identification techniques for highly boosted W bosons that decay into hadrons*, *JHEP* **12** (2014) 017, [1410.4227].

[6] Rikkert Frederix and Stefano Frixione, *Merging meets matching in mc@nlo*, *JHEP* **12** (2012) 061, [1209.6215].

[7] Emanuele Re, *Single-top wt-channel production matched with parton showers using the powheg method*, *Eur.Phys.J.* **C71** (2011) 1547, [1009.2450].

[8] John M. Campbell, R. Keith Ellis, Paolo Nason, Emanuele Re, *Top-pair production and decay at nlo matched with parton showers*, *JHEP* **04** (2015) 114, [1412.1828].

[9] CMS collaboration, *MET POG - Recommended MET Filters for Run II - https://twiki.cern.ch/twiki/bin/view/CMS/MissingETOptionalFiltersRun2?rev=79*, .